AAPS PharmSciTech (2020) 21: 14
DOI: 10.1208/s12249-019-1561-2

Check for updates

Research Article

QbD Approach for Novel Crosslinker-Free Ionotropic Gelation of Risedronate Sodium–Chitosan Nebulizable Microspheres: Optimization and Characterization

Omar A. Elkady,[1] Mina Ibrahim Tadros,[2,3] and Hanan M. El-laithy[1,2]

Received 12 August 2019; accepted 7 November 2019; published online 5 December 2019

Abstract. Risedronate sodium (RS) is a potent inhibitor of bone resorption, having an extreme poor permeability and limited oral bioavailability (0.62%). RS should be orally administered under fasting conditions while keeping in an upright posture for at least 30 min to diminish common gastroesophageal injuries. To surmount such limitations, novel risedronate–chitosan (RS–CS) crosslinker-free nebulizable microspheres were developed adopting the quality by design (QbD) approach and risk assessment (RA) thinking. RS:CS ratio, surfactant (Pluronic® F127) concentration, homogenization duration, speed, and temperature were identified using Ishikawa diagrams as the highest formulation and process risk factors affecting the critical quality attributes (CQAs), average particle size (PS), and entrapment efficiency (EE%). The risk factors were screened using the Plackett–Burman design, and the levels of the most significant factors were optimized using a multilevel factorial design to explore the optimized system with the least PS, maximum EE%, and a prolonged drug release profile. The optimized system (B6) was developed at a RS:CS ratio of 1:7, a surfactant concentration of 2% (w/v), and a homogenization speed of 14,000 rpm. It revealed good correlation with QbD theoretical prediction, where positively charged (47.9 ± 3.39 mV) discrete, spherical microspheres (3.47 ± 0.16 μm) having a high EE% (94.58 ± 0.19%) and prolonged RS release over 12 h ($Q_{12\ h}$, 89.70 ± 0.64%) were achieved. *In vivo* lung deposition after intratracheal instillation of B6 confirmed the delivery of high RS percentage to rat lung tissues (87 ± 3.54%) and its persistence for 24 h. This investigation demonstrated the effectiveness of QbD philosophy in developing RS–CS crosslinker-free nebulizable microspheres.

KEY WORDS: risedronate sodium; crosslinker-free; chitosan; microspheres; quality by design (QbD).

INTRODUCTION

Inhalation of drugs is a way of administration which is set in motion by patients to deliver drugs to their sites of action to achieve either systemic or local effects (1,2). The pulmonary drug delivery guarantees a noninvasive route which promotes a fast rate of drug absorption due to the lung expansive surface area and the abundant capillary vessels (3,4).

Bisphosphonates (BPs) are pyrophosphate analogs which contain a phosphate–carbon–phosphate (P–C–P) backbone. They are potent inhibitors of bone resorption and are commonly used in the treatment of metabolic bone diseases such as osteoporosis, Paget's disease, and metastatic bone disease (5,6). BPs primarily exert their effects on osteoclasts *in vivo* at active bone remodeling sites and thus inhibit osteoclast-mediated bone resorption (6,7). Compared with 'simple' BPs (like etidronate and clodronate), nitrogen-containing ones (like risedronate, alendronate, and zoledronate) exhibit more potent antiresorptive effects (6). It is worth to note that strict dosing guidelines are essential for the clinical success of the current oral marketed nitrogen-containing BP products. Patients are instructed to take BPs 30 min before the first food or drink with 180–250 mL water while maintaining in an upright posture. Poor compliance can drastically hamper the drug absorption and favor the formation of insoluble nonabsorbable complexes at the absorption sites due to the strong interactions with calcium and other divalent cations in the gastrointestinal tract (8). In a parallel line, BPs at the empty stomach pH (1–2) are primarily converted to their free acid forms which are known to be more irritating to the stomach and the esophagus than their sodium salt forms (9,10). Consequently, gastroesophageal adverse effects such as epigastric pain, dyspepsia, nausea, vomiting, bleeding ulcers, and erosive esophagitis are frequently concomitant to the oral BP intake due to the reflux of

[1] Department of Pharmaceutics, Faculty of Pharmacy, October University for Modern Sciences and Arts (MSA), Giza, 11787, Egypt.
[2] Department of Pharmaceutics and Industrial Pharmacy, Faculty of Pharmacy, Cairo University, Kasr El-Aini Street, Cairo, 11562, Egypt.
[3] To whom correspondence should be addressed. (e-mail: mina.tadros@pharma.cu.edu.eg; mina_ebrahim@yahoo.com)

gastric contents containing the free acid form (8,11). In fact, applying the abovementioned guidelines is usually insufficient to avoid these side effects (12). Moreover, BPs are members of BCS class III group and have limited oral bioavailabilities (< 1%). They suffer from extreme poor transport through transcellular and paracellular routes, possibly due to their high hydrophilicity, large molecular size, and negative surface charge (12,13).

Among BPs, risedronate sodium (RS) with high antiresorptive activity was investigated in this study. RS possesses a short elimination half-life time (1.5 h) which necessitates frequent dosing and, consequently, excessive extended exposure to the gastrointestinal epithelium and poor patient compliance (14,15). A limited number of studies were conducted to surmount such limitations and to promote the systemic delivery of RS via different routes. Pazianas *et al.* developed an enteric-coated tablet containing EDTA as a chelating agent to carry RS to the small intestine with lower mineral concentrations than the stomach where the EDTA competitively forms complexes with multivalent cations instead of RS (16). Unfortunately, EDTA was responsible for more abdominal pain when taken on fasting conditions, and upon post-prandial administration, RS absorption was decreased by around 30%. Instead of EDTA, Kim *et al.* used phytic acid as a chelating agent which showed an equivalent RS release profile to the marketed tablet product (17). Different trials were investigated to minimize the drug toxic oral side effects including the development of a topical formulation of RS–polyethylene glycol nanoparticles (18) and RS–PLGA nanoparticles for intranasal delivery (15). Very few attempts were carried out to deliver RS via the pulmonary route. Nasr and coworkers developed inhalable RS–PLGA microspheres using w/o/w double emulsion technique (10) and RS–liposomes adopting reversed phase evaporation technique (12). These techniques suffer from many limitations including the lengthy/tedious production steps, the need for special equipment, the use of organic solvents, the moderate drug entrapment efficiency, and the limited scaling up possibilities. Therefore, endeavors to enhance RS delivery through formulations with less gastrointestinal adverse effects and better drug transport are still required and remain a challenge in BP delivery.

To date, chitosan (CS)-based pulmonary delivery systems were extensively used to enhance the permeation and bioavailability of many drugs (19–22). Crosslinking agents like tripolyphosphate (TPP) or glutaraldehyde (GA) have been widely applied to fabricate sustained release systems (19–24). However, valid concerns of toxic effects of glutaraldehyde exposure including respiratory epithelium hyperplasia, chronic bronchitis, respiratory tract sensitization that extend to asthma, nasal lesions, skin and eye irritation, headache, fatigue, vomiting, colitis, tachycardia, and fever have been reported (25,26).

Therefore, based on the above considerations, slow RS release is crucial to diminish the frequent dosing-related drawbacks and allow sufficient time between doses to repair the damaged epithelium if any (14). In this perspective, direct interionic complexation of CS cationic amino groups with negatively charged RS could be a suitable solution for the hindered drug transport and facilitates the opening of the epithelium tight junctions enhancing both the transcellular and paracellular pathways (27).

Quality by design (QbD) is a regulatory, systematic, risk science, and knowledge-based system with modern quality management thinking. QbD focuses on the design phase to ensure the quality of the predefined final target product (28,29). Currently, this approach is highly recommended and welcomed by the US Food and Drug Administration (FDA) and the European Medicines Agency (EMA) regulatory authorities to efficiently shorten the time needed in practice for the development of the target product with effective time management and resources allocation. QbD necessitates the determination of the quality target product profile (QTPP), critical quality attributes (CQAs) which critically affect the quality properties of the final product, and critical process parameters (CPPs) which can significantly influence the CQAs and QTPP. Scientific knowledge from previously reported literature is the basic source for the selection of CQAs and CPPs (29,30).

In this approach, risk assessment (RA) is emphasized to be the most important component and the key tool of the QbD. It is used in identifying and ranking the risk parameters that may critically affect the pre-identified COAs (31).

Herein, the direct electrostatic interaction between RS and CS was investigated, using the QbD approach, to develop safe crosslinker-free RS–CS nebulizable microspheres which can deeply reach the alveoli and provide prolonged RS release.

MATERIALS AND METHODS

Materials

Risedronate sodium hemi-pentahydrate was gifted by Sanofi (Cairo, Egypt). Low molecular weight chitosan flakes (average M_w 150 kDa, deacetylation degree ≥ 75%), Pluronic® F127, xylazine hydrochloride, ketamine hydrochloride, Triton™ X-100, tetrabutylammonium hydroxide (TBAH), sodium pyrophosphate, acetonitrile, and magnesium ascorbyl phosphate were purchased from Sigma-Aldrich (St Louis, MO, USA). Glacial acetic acid was obtained from El Nasr Pharmaceutical Chemicals Co. (Cairo, Egypt). All other chemicals were of analytical grade and used as received.

Animals

Eight-week-old male Wistar albino rats weighing 300–350 g were derived from the animal house of the Research Institute of Ophthalmology (Giza, Egypt). Rats were housed individually in stainless steel cages at 25 ± 2°C, relative humidity range of 40–60%, and 12 h light–dark cycles. Rats were provided with standard chow and drinking water *ad libitum*. Seven days were allowed for acclimatization of the rats before any progression in experimental work.

Application of Quality by Design Approach

Determination of the Quality Target Product Profile and Selection of Critical Quality Attributes

The first step in applying the QbD approach is to determine the QTPP by defining the desired product and its

features. This step usually encompasses therapeutic requirements and other quality demands that furnish a quantitative surrogate for safe and efficient clinical use like the route of administration, dosage form, particle size, dissolution profile, *etc*. Herein, the QTPP that should be ideally achieved was to develop RS–CS nebulizable microspheres which can deeply reach the alveoli with prolonged dosing intervals.

The second step in QbD methodology was to select the CQAs, based on the pre-identified QTPP and literature knowledge. CQAs are defined as the quality attributes that must be studied, controlled, and guaranteed during the product development to ensure the final product quality (QTPP). CQAs are generally associated with the excipients, the in-process materials, the drug substance, or the final product (32,33).

The particle size and the entrapment efficiency were the selected CQAs that can significantly affect the quality and efficacy of the developed RS–CS nebulizable microspheres (34). Previous reports showed microsphere systems possessing a mean particle diameter of 1–5 μm are needed to assure deep lung deposition in the alveoli by the sedimentation mechanism. Larger particles are commonly known to deposit in the oropharyngeal and bronchial regions by inertial impaction, while smaller ones are generally exhaled (35,36). Moreover, polymer-based microparticles offer potential benefits over other carriers, due to their reported higher stability, higher drug entrapment capacity, prolonged drug release, and longer pharmacological activity of payloads (36), thus allowing for prolonged dosing intervals and higher patient compliance (37,38).

Risk Assessment

Based on preliminary studies and literature knowledge, risk assessment was implemented to identify and prioritize all the high-risk material attributes and process parameters that may potentially affect RS–CS inhalable microsphere CQAs using a qualitative risk-ranking approach, thus avoiding profitless efforts in the development process (32,39).

Ishikawa (fishbone or cause-and-effect) diagrams were set up as the graphical tool for highlighting all factors that can influence the particle size and the entrapment efficiency (CQAs) of RS–CS microspheres and organizing them hierarchically (Fig. 1). Fishbone diagrams were generated using Minitab® 17 software (Minitab Inc.; State College, PA, USA) (31,37). A large number of variables from many categories, *i.e.*, materials, formulation, environment, homogenization process, methods, and measurements, *etc.*, were reported in the literature (40,41), some of which were suggested to play a vital role on CQAs affecting the development of RS–CS inhalable microspheres.

The results of the Ishikawa-based RA ascertained that RS:CS ratio, surfactant concentration, homogenization duration, speed, and temperature were the critical factors that were assessed to be of high importance compared to others. These factors could pose potential risk for particle size and entrapment efficiency and thus need further investigations to ensure quality. RA could be refined and updated at different development stages as further data becomes available and more knowledge is obtained (32). The significance of these parameters on the CQAs was determined in the screening studies keeping the uncontrollable factors like maturation time, drug concentration, and polymer concentration fixed in order to reduce redundant variability (42).

Risk Analysis: Screening Phase

Risk analysis (screening phase) is an experimental study in which RA-based high-risk factors are simultaneously and quantitatively evaluated using a fewer number of runs to indicate their degree of criticality on CQAs (32,34). Herein, Plackett–Burman, a first-order experimental model of high degree of accuracy and efficiency, was used for identifying the crucial factors and levels which should be addressed or eliminated in further investigations. The factor level selection was based on preliminary studies and literature knowledge and should not be too close or too far away from each other (38,42–44). The Plackett–Burman design was currently created using Minitab® 17 software. The RS:CS ratio, surfactant concentration, homogenization duration, and speed were screened as numerical factors, whereas the homogenization temperature was evaluated as a categorical factor. All factors were investigated at two levels (low and high). To evaluate the potential curvature, two center points were added and a total of 14 runs were attempted. The particle size (PS) and the drug entrapment efficiency (EE%) were the CQAs (Table I).

Preparation of RS–CS Microspheres

RS–CS microspheres were prepared by the ionotropic gelation technique (24,45), yet without the addition of a crosslinker like TPP. The spontaneous development of RS–CS microspheres was based on the electrostatic interaction between RS anionic solution and CS cationic solution.

CS solution (1%, w/v) was prepared by dispersing CS flakes in acetic acid solution (1% v/v) and stirring at 450 rpm (Stuart magnetic stirrer, Bibby Scientific Ltd, UK) at room temperature till complete dissolution. RS solution (1%, w/v) was developed by dissolving RS in aqueous solutions of different Pluronic® F127 concentrations [0.5, 1 (center point), and 1.5%, w/v]. Seven runs of RS–CS microspheres were developed by drop-wise addition of RS–surfactant solution to CS solution while homogenization (Silent Crusher M homogenizer, Heidolph, Germany) so that drug:polymer ratios were 1:1, 1:3 (center point), and 1:5. The homogenization speed was varied at 5000, 8000 (center point), and 11,000 rpm for 1, 3 (center point), and 5 min at room temperature (25 ± 1°C). The resulting dispersions were concentrated to the required volumes (containing 5 mg RS) and the formed microspheres were obtained by centrifugation (Heraeus Megafuge 16R, Hanau, Germany) at 15,000 rpm and 4°C for 1 h. The collected microspheres (the sediment) were washed with deionized water, filtered, dried at 40°C for 24 h, and finally stored in a desiccator for further use. Parallel set of runs was similarly conducted while surrounding the homogenizer with an ice bath. The composition of the developed RS–CS microspheres is summarized in Table I.

Optimization Phase

Based on the screening phase results, three critical factors (RS:CS ratio, surfactant concentration, and

homogenization speed) were promoted to the optimization phase, using the response surface method and a multilevel factorial design to accurately and precisely investigate the effects of each critical factor at different levels on the CQAs (38,46). Accordingly, RS:CS ratio and surfactant concentration were tested at two levels of (1:3 and 1:7) and (1 and 2% w/v), respectively. On the other hand, the homogenization speed was tested at four levels (8000, 11,000, 14,000, and 17,000 rpm). The homogenization duration and temperature were fixed at 5 min and room temperature, respectively, since these conditions were found to be optimum (47). The levels were selected so as to reduce the probability of missing the optimum effect, by setting the corresponding center points in Plackett–Burman design of the three factors as low levels in the multilevel factorial design, while higher levels than the previously examined in the screening phase were selected as their upper extreme levels (42).

After careful reconsideration of CQAs, the RS release percentages after 1 h ($Q_{1\ h}$) and 12 h ($Q_{12\ h}$) were added as additional responses in the optimization design and were considered to be as important as PS and drug EE% (43).

The optimized system was selected by setting the desirability criteria of attaining the least PS values, the maximum EE%, the minimum $Q_{1\ h}$, and the highest $Q_{12\ h}$. Minitab 17® software was the technical tool used for creating and analyzing the multilevel factorial design and plotting a series of surface and contour graphs (37).

Verification Phase

In order to establish the reliability and to prove the validity of the optimization design, the factor settings with optimal results had to be repeated. Therefore, the optimized system (B6) was reprepared and recharacterized, whereby magnitude of error between the previous and the current prepared runs was assessed (31,37).

Characterization of RS–CS Nebulizable Microspheres

Particle Size Analysis

The mean particle size and size distribution of the prepared systems were determined using a Malvern Mastersizer 2000 laser diffraction particle size analyzer operated with Malvern Mastersizer software version 5.61 (Malvern Instruments Ltd., Worcestershire, UK). Each system was placed in a wet sample dispersion unit, diluted with distilled water (refractive index 1.33), and stirred to keep the sample dispersed while the particle size was being measured, so that the laser obscuration was kept above 5%. Data for each measurement was collected for 12 s (12,000 snaps). All measurements were performed in triplicates.

Determination of Drug EE%

The drug EE% was determined using an indirect method. Briefly, 1 mL of the RS–CS microsphere dispersion was centrifuged at 15,000 rpm and 4°C for 1 h. The supernatant was filtered using 0.45 μm microfilter and analyzed spectrophotometrically after appropriate dilution at 262 nm (UV-1601 PC, Shimadzu, Japan), according to the following equation:

$$\mathrm{EE\%} = \left(\frac{\text{Amount of total drug} - \text{Amount of drug in the supernatant}}{\text{Amount of total drug}}\right) \times 100$$

The absorbance measurement was carried out using a pair of matched Quartz cuvettes (path length = 1 cm) with phosphate buffered saline (PBS) solution (pH 7.4, 0.154 mM) in a blank cell. The zero-order absorption spectra (D^0) of RS was recorded in the range of 200–400 nm where it exhibited a λ_{max} at 262 nm (12). The concentration of RS was calculated from the previously constructed calibration curve. The linear range was 0.5–80 μg/mL; good linearity was ascertained by the correlation coefficient values approaching the value of 1. The accuracy of the method was accomplished at five concentration levels, while the precision was established from three different concentration levels through triplicate analysis of each concentration. Good accuracy was ascertained by the values of the recovery percentage obtained (98–102%), while good precision confirmed as the relative standard deviation (RSD) for the results was usually less than 2%.

In Vitro Drug Release Studies

No pharmacopeial method is applicable for the determination of sustained drug release to the lung (48). The *in vitro* release studies of RS from its aqueous solution and from RS–CS microspheres were performed using the method reported by Salama *et al.* (49). Franz diffusion cell (Hanson research, Los Angeles, CA, USA) with a diffusion area of 1.77 cm^2 was used. The receptor compartment contained 7.5 mL of PBS solution (pH 7.4, 0.154 mM) maintained at 37°C by a circulating water jacket and was constantly stirred at 150 rpm with a small magnetic bar. RS aqueous solution and RS–CS microspheres containing equivalent to 5 mg of RS were dispersed in 200 μL PBS and placed in a semipermeable membrane tubing (12,000–14,000 molecular weight cutoff, presoaked overnight in PBS, pH 7.4), tightly fitted from both sides, and loaded into the receptor compartment. At certain time intervals (0, 0.25, 0.5, 1, 2, 3, 4, 5, 6, 8, and 12 h), 0.5 mL samples were aliquoted from the receptor compartment and replaced with equal volumes of fresh medium. The amount of drug released was determined spectrophotometrically at 262 nm. For comparative studies, the drug release percentages after 1 h ($Q_{1\ h}$) and 12 h ($Q_{12\ h}$) were determined.

Transmission Electron Microscopy

The morphological characteristics of the optimized system (B6) were examined using transmission electron microscopy (TEM). One drop of the microsphere dispersion was loaded on the carbon-coated copper grid (200 mesh) and negatively stained with 1% aqueous solution of phosphotungestic acid, and the excess was drawn off using a filter paper. The sample was dried at room temperature and examined using JEM-2100 high-resolution transmission electron microscope (Jeol, Tokyo, Japan) at an acceleration voltage of 80 kV under different magnification powers.

Zeta Potential Measurement

The zeta potential (ζ) of the B6 system was determined according to the electrophoretic light scattering (ELS) technology using a Laser Doppler Anemometer coupled with a Zetasizer Nano ZS (Malvern Instruments Ltd., Worcestershire, UK). Measurements were carried out in triplicate at 25 ± 1°C and the zeta potential values were calculated from the mean electrophoretic mobility values using the Helmholtz–Smoluchowski equation built into the Malvern Zetasizer software (50).

X-ray Diffraction

X-ray diffraction (XRD) spectra were recorded at room temperature for pure RS, CS, RS–CS physical mixture, and the lyophilized B6 system using Siemens D5005 diffractometer with Cu-Kα radiation generated at 40 mA and 35 kV. Samples were analyzed in a 2θ range of 3–60° with a step size of 0.02° and a counting time of 0.4 s per step.

Fourier Transform Infrared Spectroscopy

In order to determine the chemical interactions between RS and CS, the Fourier transform infrared spectroscopy (FT-IR) spectra showing the structural changes in the RS–CS lyophilized optimized system were recorded using IRAffinity-1 Fourier transform infrared spectrometer (Shimadzu, Kyoto, Japan) over the range of 400–4000 cm^{-1}. Potassium bromide pellets containing the samples were prepared prior to FT-IR analysis (2 mg sample/300 mg KBr) (51).

***In Vivo* Lung Deposition Study**

RS content in the lung tissues of rats was determined after intratracheal instillation of RS–CS optimized system (B6) according to the method adopted by Stubbs *et al.* and Fan *et al.* with slight modifications (52,53). The protocol of the study was reviewed and approved by the Research Ethics Committee (PI 1583) at the Faculty of Pharmacy, Cairo University (Cairo, Egypt). The animals were anesthetized with xylazine (10 mg/kg) and ketamine hydrochloride (100 mg/kg) intraperitoneal injection. A volume of B6 system equivalent to 0.5 mg/kg of RS was administered intratracheally to the rats using a model 1A-1B Micro-Sprayer® aerosolizer (Penn Century Inc., Wyndmoor, PA, USA). Rats were sacrificed, 24 h post-administration, under general anesthesia. Lungs were collected after separation from the attached organs (heart, vessels, and thymus) under a microscope and homogenized in PBS solution (pH 7.4, 0.154 mM) containing 0.1% Triton™ X-100 for lysing cells. The homogenates were subjected to lyophilization where 10 mg of the lyophilized lung was treated by PBS, transferred to centrifuge tubes, and centrifuged at 16,000 rpm for 5 min (54). The supernatants were collected and analyzed for RS using the HPLC method previously reported by Kyriakides and Panderi (55) using an Agilent 1100 HPLC system (Agilent Technologies, Santa Clara, CA, USA) with a UV detector (Agilent VWD G1314A). Chromatographic separation was carried out on Nova-Pak C18 column (5 mm, 4.6 mm × 150 mm; Waters, Milford, MA, USA) at ambient temperature. The mobile phase consisted of 0.005 M tetrabutyl ammonium hydroxide and 0.005 M sodium pyrophosphate (pH 7.0) mixed with acetonitrile in a ratio (78:22, v/v). The flow rate was set at 1 mL/min with a column inlet pressure of 1350 psi in order to separate RS and magnesium ascorbyl phosphate (internal standard) and the detection was carried out at 262 nm.

RESULTS AND DISCUSSION

Risk Analysis: Screening Phase

RS–CS systems were prepared—as described above—in compliance with the Plackett–Burman design to screen the effects of RS:CS ratio (X1), surfactant concentration (X2), homogenization speed (X3), duration (X4), and temperature (X5) on CQAs and PS (Y1) and EE% (Y2) to determine the most critical factors that should be addressed in further investigations. The experimental runs for the tested systems with their corresponding responses are presented in Table I.

A wide particle size distribution was obtained, ranging from 6.68 ± 0.04 μm (A10) to 40.76 ± 0.13 μm (A1). The ANOVA results revealed that, out of the five investigated factors, both the surfactant concentration and homogenization speed have significantly contributed ($P < 0.05$) to the particle size in an inverse proportional manner (Fig. 2). This finding was illustrated in the linear regression equation representing the model—after elimination of nonsignificant terms (56)—as follows:

$$Y1 = 111.6 - 202.9\,X2 - 0.000099\,X3 + 101.7\,X2^2$$

where positive and negative signs before a coefficient indicate a direct or inverse effect on the tested response, respectively. This trend could be attributed to the fact that high surfactant concentration stabilizes the RS–CS microspheres by forming a steric barrier on their surface, thus avoiding particle aggregation (37). Additionally, Pluronic® F127 is well-known as a deaggregating hydrosoluble surfactant which is able to swell after hydration to facilitate the disintegration of the produced particles, thus favoring the formation of smaller microspheres (57,58). In a parallel line, high homogenization speed promotes proper mixing and better dispersion with surfactant due to the high shear forces produced; therefore, a decrease in particle agglomeration and size diameter was observed (59,60).

Interestingly, all the prepared systems successfully entrapped RS efficiently with EE percentages ranging from 87.84% (A14) to 99.59% (A8) as evident from Table I. ANOVA results revealed that RS:CS ratio was the only significant factor ($P < 0.05$), while the other four factors were nonsignificant (Fig. 2). The fitted linear regression equation to EE% (Y2) is given below:

$$Y2 = 91.93 + 1.118X1$$

where EE% is directly correlated to CS content in the microspheres.

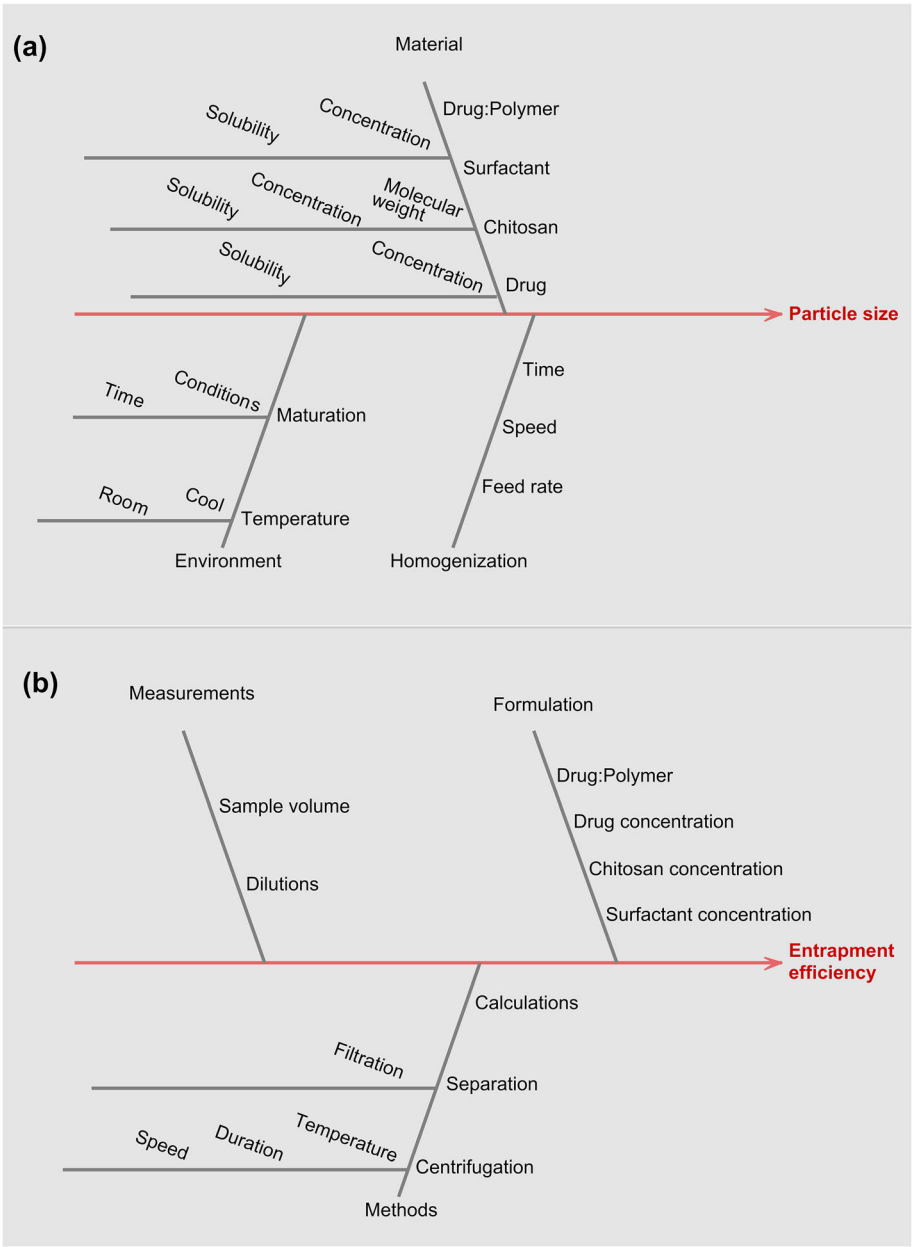

Fig. 1. Ishikawa diagrams for **a** particle size and **b** entrapment efficiency

Based on the risk analysis results, only the significant factors (RS:CS ratio, surfactant concentration, and homogenization speed) were promoted to the optimization phase using a more predictive response surface model, while the other nonsignificant factors (homogenization duration and temperature) were fixed at 5 min and room temperature (25 ± 1°C), respectively.

Optimization Phase

In the optimization phase, a more predictive multilevel factorial design was performed to analyze more accurately and precisely the effects of the significant factors (X1: RS:CS ratio, X2: surfactant concentration, and X3: homogenization speed) and their interactions on four responses (Y1: particle size, Y2: EE%, Y3: $Q_{1\ h}$, and Y4: $Q_{12\ h}$). It is worth to note that RS release percentages after 1 and 12 h were added to the optimization design in order to explore the capability of CS to sustain RS release and to prolong its residence time in the lungs. Sixteen experimental runs were conducted, and their results are shown in Table II.

Effect on Particle Size (Y1) and Entrapment Efficiency (Y2)

Similar to the results of Plackett–Burman screening, significant inverse relationships were only established between both the surfactant concentration and the homogenization speed (P value = 0.0001 and 0.003, respectively) and the mean observed particle size, without a significant interaction effect between these two key parameters X2 and X3 (P value = 0.839). The surface plot (A) in Fig. 3 revealed a marked reduction in the particle size with the gradual

Table I. Plackett–Burman Design for Screening the High-Risk Factors (X1–X5)

System	Numerical factors				Categorical factor	CQAs	
	X1: RS:CS (ratio)	X2: surfactant conc. (% w/v)	X3: homogenization speed (rpm)	X4: homogenization duration (min)	X5: homogenization temperature	Y1: particle size (μm)	Y2: EE (%)
A1	1:1	0.5	11,000	5	Room	40.76 ± 0.13	92.87 ± 0.42
A2	1:1	1.5	11,000	5	Room	30.77 ± 0.25	98.70 ± 0.36
A3	1:1	0.5	5000	1	Room	40.05 ± 0.07	92.49 ± 0.54
A4	1:5	0.5	5000	5	Cool	39.63 ± 0.28	98.68 ± 0.27
A5	1:5	1.5	5000	5	Room	36.14 ± 0.18	98.75 ± 0.43
A6	1:5	1.5	11,000	1	Cool	38.66 ± 0.24	99.31 ± 0.17
A7	1:1	1.5	5000	5	Cool	36.04 ± 0.32	96.08 ± 0.41
A8	1:5	0.5	5000	1	Room	31.16 ± 0.22	99.59 ± 0.26
A9	1:1	1.5	5000	1	Cool	20.99 ± 0.08	92.30 ± 0.51
A10	1:3	1	8000	3	Room	6.68 ± 0.04	95.39 ± 0.17
A11	1:5	1.5	11,000	1	Room	34.54 ± 0.42	97.61 ± 0.21
A12	1:5	0.5	11,000	5	Cool	21.82 ± 0.1	94.84 ± 0.31
A13	1:1	0.5	11,000	1	Cool	32.02 ± 0.16	89.51 ± 0.37
A14	1:3	1	8000	3	Cool	9.58 ± 0.09	87.84 ± 0.15

CQAs (Y1–Y2) are expressed as mean values ± SD, $n = 3$
CQAs critical quality attributes, *RS* risedronate sodium, *CS* chitosan, *EE* entrapment efficiency

increase in the surfactant concentration and the homogenization speed up to their upper extreme limits (2% w/v and 17,000 rpm, respectively). Interestingly, it could be inferred from Table II that regardless of the RS:CS ratio, a successful particle size range for deep lung deposition (1–5 μm) could be achieved in the systems (B4, B6, B9, and B15) prepared with high surfactant concentration (2% w/v) while using high homogenization speeds (14,000 and 17,000 rpm) only. The following regression equation below confirmed the obtained results.

$$Y1 = 11.20 + 5.65\,X2_1 - 5.65\,X2_2 + 7.84\,X3_{8000} + 0.68\,X3_{11,000} - 3.80\,X3_{14,000} - 4.71\,X3_{17,000}$$

The opposite was held true for the EE%. All the investigated independent factors (X1, X2, and X3) as well as their interaction effects were significant ($P < 0.05$). The systems prepared with upper RS:CS ratio level (1:7) showed higher EE% than those attained at the lower level (1:3) (Table II). These findings stem from the fact that high CS concentration would favor the electrostatic interaction between its positively charged amino groups and the negatively charged RS molecules leading to the formation of a polyelectrolytic complex. The increase in the CS concentration would lead to a more compact microsphere structure which is expected to hamper the diffusion of the drug and contribute to a more effective drug entrapment (46,61). Likewise, the surfactant concentration contributed positively to the EE%. Microspheres prepared with a 2% w/v surfactant concentration (B11, B14, B6, B4, and B7) showed higher EE% than their corresponding ones prepared with the lower surfactant concentration (B2, B12, B5, B3, and B10), respectively. This could be assigned to the increased number of the developed micelles at high Pluronic® F127 concentrations which promoted the development of more rigid and entangled systems (62). As revealed in Fig. 3, the homogenization speed had a negative impact on drug EE%. The corresponding values of the systems (B6, B7, B9, B11) could be arranged in the following descending order B11 > B7 > B6 > B9 with the increase in the homogenization speed from 8000 to 17,000 rpm. This trend could be understood if one considers the formation of smaller microspheres with the increase of the homogenization speed which allows for drug diffusion out before the complete formation of microspheres and, thus, decreases the drug EE% (63).

The regression equation of EE% (Y2) model is:

$$\begin{aligned} Y2 = {} & 91.72 - 1.72\,X1_3 + 1.72\,X1_7 - 4.62\,X2_1 + 4.62\,X2_2 \\ & + 0.81\,X3_{8000} + 3.68\,X3_{11,000} - 2.33\,X3_{140,00} \\ & - 2.16\,X3_{17,000} - 2.82\,X1_3X2_1 + 2.82\,X1_3X2_2 \\ & + 2.82\,X1_7X2_1 - 2.82\,X1_7X2_2 - 2.75\,X1_3X3_{8000} \\ & + 4.69\,X1_3X3_{11,000} + 0.46\,X1_3X3_{14,000} \\ & - 2.40\,X1_3X3_{17,000} + 2.75\,X1_7X3_{8000} \\ & - 4.69\,X1_7X3_{11,000} - 0.46\,X1_7X3_{14,000} \\ & + 2.40\,X1_7X3_{17,000} - 0.72\,X2_1X3_{8000} \\ & + 2.84\,X2_1X3_{11,000} - 1.68\,X2_1X3_{14,000} \\ & - 0.44\,X2_1X3_{17,000} + 0.72\,X2_2X3_{8000} \\ & - 2.84\,X2_2X3_{11,000} + 1.68\,X2_2X3_{14,000} \\ & + 0.44\,X2_2X3_{17,000} \end{aligned}$$

These equations consisted of the coefficients for intercept, first-order main effects, and interaction terms. The main effects of $X1_3$, $X2_1$, and $X3_{8000}$ indicate the relative influence of each factor at a certain level on the response, *i.e.*, average result of changing one variable at a time from its low to its high level. The interaction terms ($X1_3X2_1$, $X1_3X3_{8000}$, and $X2_1X3_{8000}$) show how the response changes when two variables are simultaneously changed at each level. ANOVA results and fit statistics (following Box–Cox transformation) are summarized in Table III.

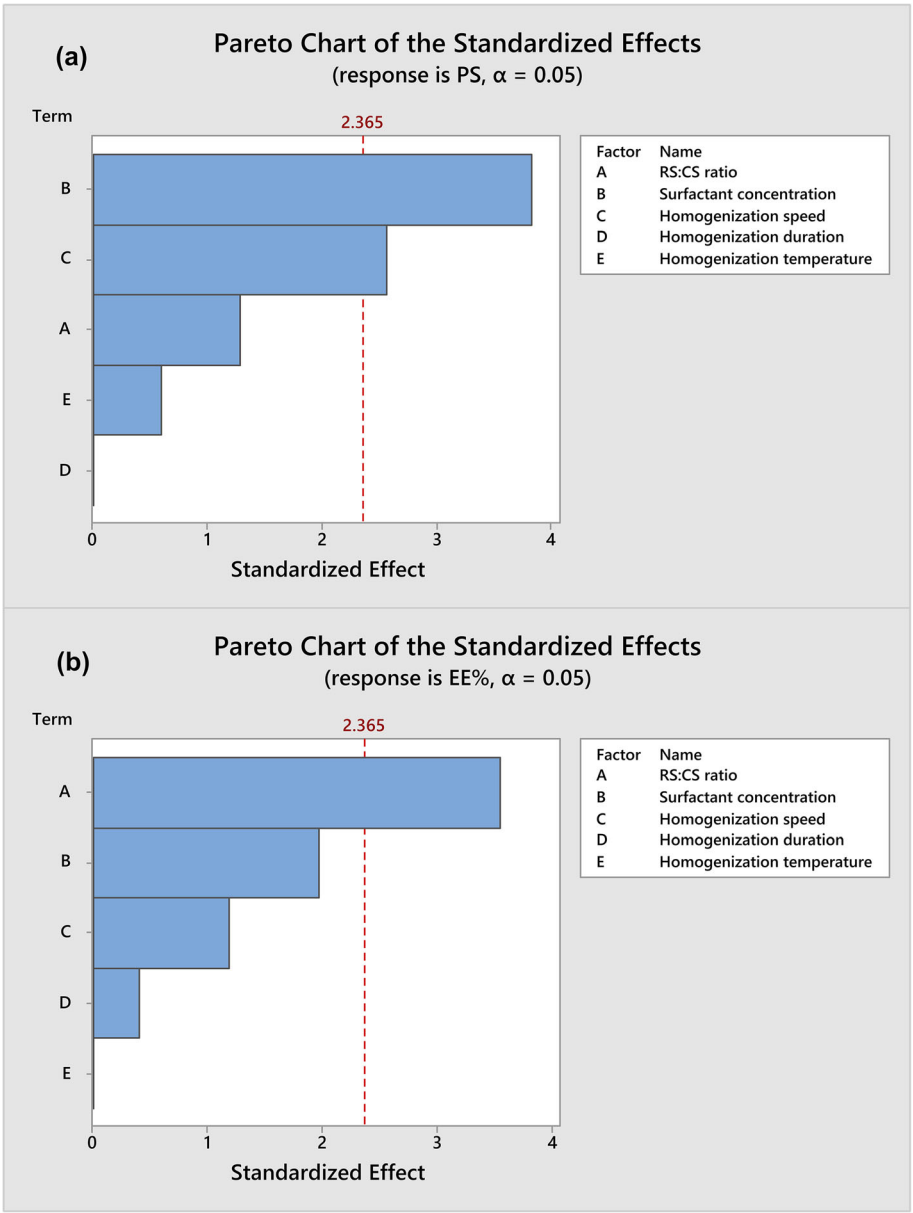

Fig. 2. Pareto charts of Plackett–Burman screening design demonstrating the influence of each factor on **a** particle size and **b** EE% responses

Effect on RS Release Percentage (Y3 and Y4)

The respiratory tract has a large surface area of $>100\ m^2$ and contains $\approx 1\ \mu L/cm^2$ of liquid (generally endogenous phospholipids and mucus) which forms a thin film lining the airways. Consequently, the evaluation of the dissolution profile of an inhalable drug in a large volume may lack a well *in vitro–in vivo* correlation. Therefore, the Franz diffusion cell approach was used, in the current work, as an alternative to conventional dissolution testing apparatus (49).

The cumulative RS release percentages as a function of time from RS–CS microspheres and the plain RS aqueous solution (as a control) were compared. As shown in Fig. 4, plain RS solution showed a rapid diffusion of ≈ 90% of the drug in 15 min only indicating complete loss of the drug in a very short period of time. Perversely, a biphasic RS release pattern was generally observed with RS–CS systems and characterized with an initial burst release in 1 h followed by a slower progression of up to ≈ 94% in 12 h. This pattern is advantageous as the initial rapid drug release phase can help to achieve high RS plasma concentration in the lungs in a short time, while the sustained release phase would be expected to provide successful drug delivery for a prolonged period, which was vital to diminish the drawbacks related to RS frequent dosing. The former phase can be attributed to RS fraction adsorbed or weakly bounded to the surface of CS (64). In the latter phase, the principal pathway of drug release is controlled by drug diffusion from the core of the microspheres across the polymer matrix. Generally, the hydrophilicity of both chitosan and RS plays an important role in attracting the aqueous phase into the polymer matrix, resulting in polymer swelling and/or erosion (24). The water

Table II. Multilevel Factorial Design for Optimizing the Factors (X1–X3) Influencing RS–CS Inhalable Microspheres

System	X1: RS:CS ratio	X2: surfactant concentration (% w/v)	X3: homogenization speed (rpm)	Y1: particle size (μm)	Y2: EE%	Y3: $Q_{1\ h}$ (%)	Y4: $Q_{12\ h}$ (%)
B1	1:3	1	17,000	10.34 ± 0.12	74.55 ± 1.54	55.03 ± 2.27	61.65 ± 2.13
B2	1:7	1	8000	21.39 ± 0.07	95.99 ± 0.13	25.44 ± 1.89	75.20 ± 2.01
B3	1:3	1	14,000	12.94 ± 0.04	79.46 ± 0.58	47.87 ± 2.78	86.84 ± 0.94
B4	1:3	2	14,000	2.83 ± 0.03	96.82 ± 0.17	23.79 ± 3.14	55.37 ± 1.58
B5	1:7	1	14,000	10.33 ± 0.09	86.73 ± 0.87	39.09 ± 0.78	94.35 ± 0.77
B6	1:7	2	14,000	3.47 ± 0.16	94.58 ± 0.19	27.72 ± 1.55	89.70 ± 0.64
B7	1:7	2	11,000	5.59 ± 0.04	95.46 ± 0.08	25.49 ± 1.41	59.82 ± 0.74
B8	1:7	1	17,000	9.41 ± 0.09	94.43 ± 0.03	28.94 ± 0.56	72.16 ± 1.54
B9	1:7	2	17,000	1.90 ± 0.06	92.94 ± 0.18	31.65 ± 0.63	63.17 ± 2.99
B10	1:7	1	11,000	16.01 ± 0.07	89.41 ± 0.14	34.44 ± 0.88	56.58 ± 2.74
B11	1:7	2	8000	8.56 ± 0.13	98.01 ± 0.12	16.46 ± 2.56	75.08 ± 0.84
B12	1:3	1	8000	36.56 ± 0.05	78.40 ± 1.41	50.22 ± 1.74	77.46 ± 0.78
B13	1:3	2	11,000	8.81 ± 0.13	98.92 ± 0.07	15.47 ± 2.25	71.44 ± 1.57
B14	1:3	2	8000	9.62 ± 0.08	97.74 ± 0.06	19.40 ± 1.55	66.45 ± 2.14
B15	1:3	2	17,000	4.30 ± 0.07	96.32 ± 0.15	24.79 ± 2.27	78.23 ± 0.99
B16	1:3	1	11,000	17.78 ± 0.09	97.83 ± 0.1	20.87 ± 0.82	76.58 ± 1.27

Responses (Y1–Y4) are expressed as mean values ± SD, $n = 3$
RS risedronate sodium, *CS* chitosan, *EE* entrapment efficiency

inside the matrix enhances the disintegration of the polymer into soluble oligomeric and monomeric products. This created a passage for the drug release by diffusion and erosion until complete polymer solubilization (15,22,64). Moreover, it is rather interesting to point out that the mechanism of RS detachment from the electrostatic developed CS microspheres is pH-dependent (65). In the diluted acetic acid preparation media (pH ~ 3.56), both RS and CS were existing in their ionized forms. Single and double negative charged RS forms were formed due to deprotonation of three P–OH groups and protonation of the nitrogen atom in the pyridinium ring (66,67). Concurrently, CS under the same pH was strongly positively charged due to protonation of CS amino groups (NH_3^+) (68) leading to strong dominated ionic crosslinking between positively charged CS and negatively charged RS counterion (69). On the contrary, when the microspheres were exposed to the physiological pH (alkaline PBS release medium of pH 7.4), although RS is expected to be completely ionized and still negatively charged at pH 7.4 (70), yet, CS deprotonation took place and the fraction of protonated CS amino groups decreased dramatically, and therefore, the electrostatic interactions did not play their part (71,72) leading to low dense, degradable, and porous CS microspheres for RS liberation (69).

In the current work, high drug release percentages (≈ 55, 48, and 50%) were evident in the first hour with those systems (B1, B3, and B12) prepared with low surfactant concentration (1%) and low CS concentration (RS:CS ratio of 1:3, respectively). This could point out the significant ($P < 0.05$) positive impacts of CS and surfactant concentrations and their interactions on the drug liberation profile as expressed in the following $Q_{1\ h}$ regression equation:

$$\begin{aligned} Y3 = 30.42 &+ 1.76\ X1_3 - 1.76\ X1_7 + 7.32\ X2_1 - 7.32\ X2_2 - 2.54\ X3_{8000} \\ &- 6.35\ X3_{11,000} + 4.20\ X3_{14,000} + 4.69\ X3_{17,000} + 4.00\ X1_3X2_1 \\ &- 4.00\ X1_3X2_2 - 4.00\ X1_7X2_1 + 4.00\ X1_7X2_2 + 5.17\ X1_3X3_{8000} \\ &- 7.66\ X1_3X3_{11,000} - 0.55\ X1_3X3_{14,000} + 3.04\ X1_3X3_{17,000} \\ &- 5.17\ X1_7X3_{8000} + 7.66\ X1_7X3_{11,000} + 0.55\ X1_7X3_{14,000} \\ &- 3.04\ X1_7X3_{17,000} \end{aligned}$$

Moreover, it is clear that the increase in CS concentration, RS:CS ratio of 1:7, would elongate the diffusion path length and, hence, more sustained drug release profiles. The possible explanation for these findings could be substantiated by the fact that the increase in CS concentration would increase the viscosity of the system, trigger the precipitation of CS in the internal microsphere structure, and thus, minimize the drug diffusion through the CS matrix and hinder its loss (63). Moreover, the development of more entangled and rigid systems, due to the formation of increased number of micelles with high surfactant

Table III. Summary of ANOVA Results and Fit Statistics for the Multilevel Factorial Design Studied Responses (Y1–Y4)

Response	Lack of fit (*P*—LOF)	*P* value of the model	The correlation coefficient (R^2)	Predicted R^2	Adjusted R^2	Standard deviation (SD)
Y1	0.767	< 0.0001	0.9228	0.8413	0.8828	0.268576
Y2	0.820	0.003	0.9962	0.8926	0.9811	2.95896
Y3	0.736	0.015	0.9877	0.7492	0.9383	0.0010460
Y4	0.667	0.009	0.9917	0.7634	0.9584	7.48594

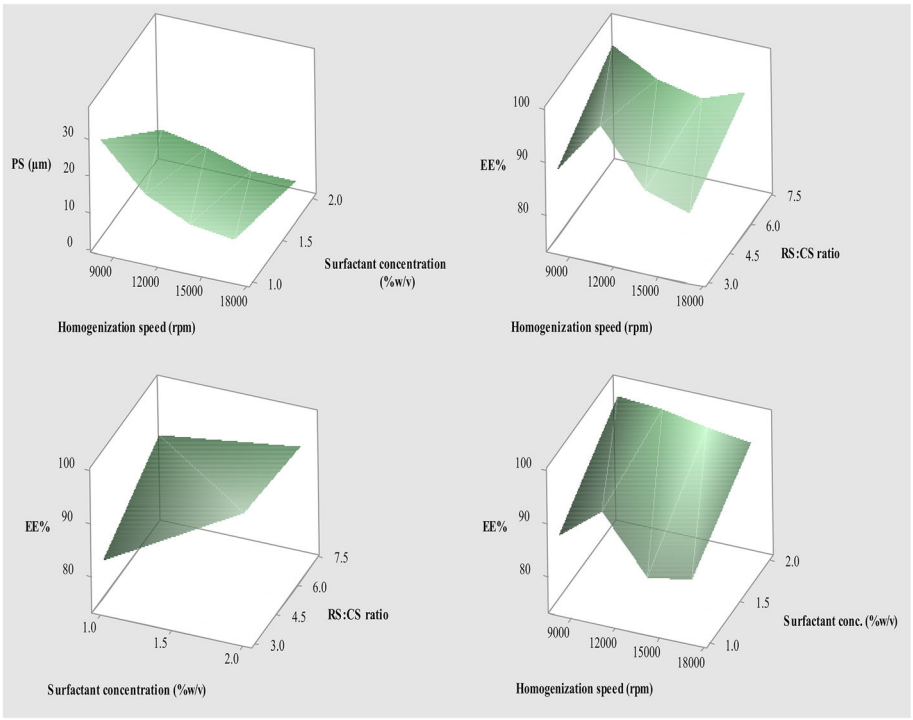

Fig. 3. 3D response surface plots of particle size and EE%

concentrations, would additionally contribute to the slowing down of the drug release profiles.

Concurrently, it could also be inferred from Table II and Fig. 5b, c, e, and f that there is a direct correlation between the drug release rates and the homogenization speed. This could be explained with reference to the decrease in the thickness of the boundary layer at the surface of the microsphere by the increase in the homogenization speed. Moreover, the disentangled micelles accumulating at the surface of the microspheres are removed faster at higher speeds. A similar observation was reported previously by Moore *et al.*, and the pattern behavior of the studied factors on RS release was well correlated with EE% results (62).

$$\begin{aligned} Y4 = {} & 72.51 - 0.75\,X1_3 + 0.75\,X1_7 + 2.60\,X2_1 - 2.60\,X2_2 + 1.04\,X3_{8000} \\ & - 6.40\,X3_{11,000} + 9.06\,X3_{14,000} - 3.70\,X3_{17,000} - 0.84\,X1_3X3_{8000} \\ & + 8.66\,X1_3X3_{11,000} - 9.71\,X1_3X3_{14,000} + 1.89\,X1_3X3_{17,000} \\ & + 0.84\,X1_7X3_{8000} - 8.66\,X1_7X3_{11,000} + 9.71\,X1_7X3_{14,000} \\ & - 1.89\,X1_7X3_{17,000} + 0.19\,X2_1X3_{8000} - 2.12\,X2_1X3_{11,000} \\ & + 6.43\,X2_1X3_{14,000} - 4.50\,X2_1X3_{17,000} - 0.19\,X2_2X3_{8000} \\ & + 2.12\,X2_2X3_{11,000} - 6.43\,X2_2X3_{14,000} + 4.50\,X2_2X3_{17,000} \end{aligned}$$

Consequently, the desirability values were calculated and the multiresponse optimization is performed using the response optimizer function inbuilt in Minitab® software to

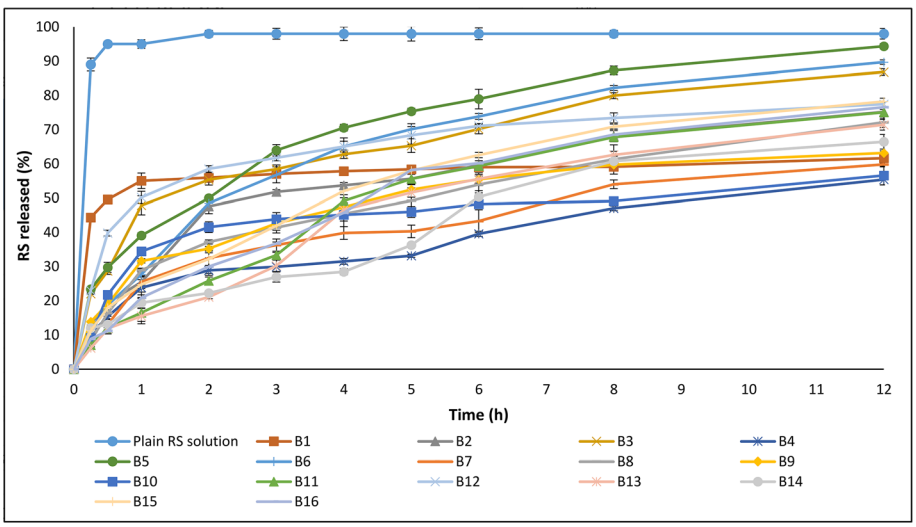

Fig. 4. *In vitro* release profiles of plain RS aqueous solution and the multilevel factorial design-derived systems

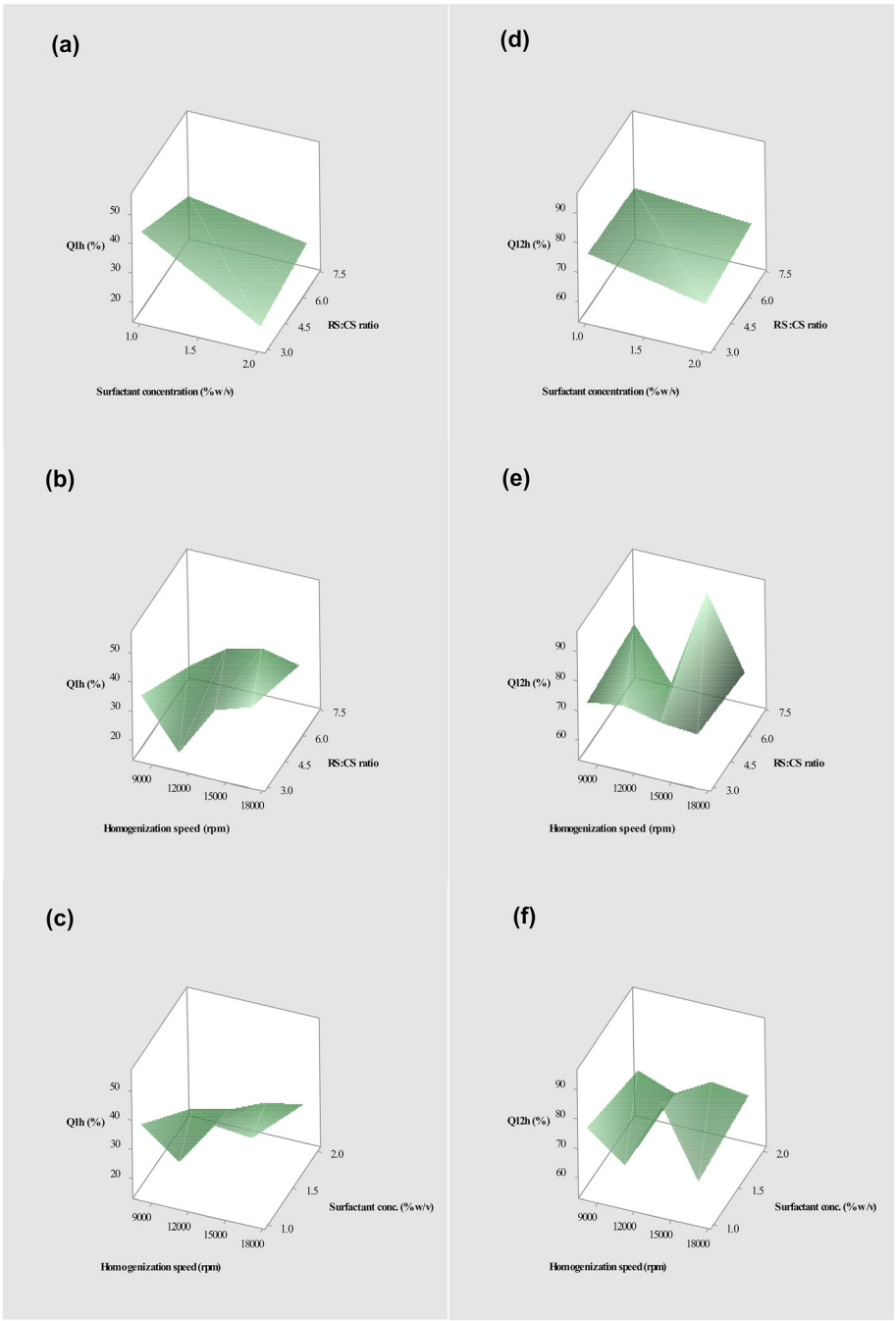

Fig. 5. 3D response surface plots of $Q_{1\ h}$ (**a–c**) and $Q_{12\ h}$ (**d–f**) responses

simultaneously optimize the levels of the independent variables (RS:CS ratio, surfactant concentration, and homogenization speed) aiming to reach the QTPP of RS–CS microspheres characterized with minimum particle size, maximum EE%, minimum $Q_{1\ h}$, and maximum $Q_{12\ h}$ (73).

Desirability in the response optimizer suggests the best combination of factor levels that satisfy the target defined for the multiple responses. Desirability index (D) has a range between 0 and 1, where 1 is the most desirable case and 0 is certainly undesirable. Individual desirability indicates how well single response is satisfied, whereas composite desirability indicates how the requirements for multiple responses are satisfied simultaneously. The four responses (Y1, Y2, Y3, and Y4) were concurrently optimized by multiresponse analysis using Derringer's desired function methodology (74). If the maximization of a response y is required, the individual desirability (d) is given by the following equation:

$$d = \begin{cases} 0 \text{ if } y \le y^{\min} \\ \left(\frac{y - y^{\min}}{y^{\max} - y^{\min}}\right) \text{if } y^{\min} \le y \le y^{\max} \\ 1 \text{ if } y \ge y^{\max} \end{cases}$$

If the minimization of the response (y) is anticipated, the equation would be:

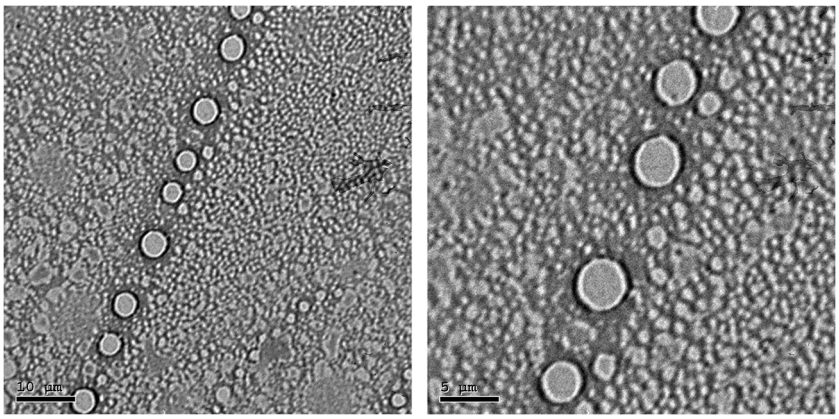

Fig. 6. TEM micrographs of the B6 system

$$d = \begin{cases} 1 \text{ if } y \le y^{\min} \\ \left(\frac{y^{\max} - y}{y^{\max} - y^{\min}}\right) \text{if } y^{\min} \le y \le y^{\max} \\ 0 \text{ if } y \ge y^{\max} \end{cases}$$

where y is the response value and $y^{\min}$ and $y^{\max}$ are the lower- and upper-bound limit of the response, respectively. When multiple responses are required, therefore, individual desirability index must be calculated for each response, then a composite desirability (D) is defined as the weighted geometric mean of all individual desirability indices normalized by the number of responses (75), determined as follows:

$$D = \left(\prod_{i=1}^{n} d_i^{w_i}\right)^{1/n}$$

where n is the number of responses and w_i are relative importance weights of different responses (the weights must add up to 1). In this study, four equally important criteria were set for optimal microsphere selection, and equal weight for each response during the optimization analysis was assumed and was set to ¼ (76,77). Therefore, in view of the aforementioned results, the B6 system was selected as the optimized system with a desirability value of 0.774 where the optimal calculated levels were RS:CS ratio (X1) = 1:7, surfactant concentration (X2) = 2% w/v, and homogenization speed (X3) = 14,000 rpm.

The experimental and predicted responses for the optimized B6 system were $Y1_{Experimental}$ 3.47 µm ($Y1_{Predicted}$, 1.74 µm; error 2.59%), $Y2_{Experimental}$ 94.58% ($Y2_{Predicted}$, 94.13%; error, 5.5%), $Y3_{Experimental}$ 27.72 ($Y3_{Predicted}$, 30.08; error, −5.33%), and $Y4_{Experimental}$ 89.70% ($Y4_{Predicted}$, 83%; error, 8.56%) (Table II). With this configuration, the B6 system provides a high degree of closeness between the responses and the target data.

To ascertain the RS release behavior from the B6 system, the release data was fitted to various release kinetic models: zero-order, first-order, Higuchi diffusion and Hixson–Crowell and Korsmeyer–Peppas models, and the coefficient of correlation (R^2) was calculated. Based on the highest R^2 value of 0.982, the release data were best fitted to the Korsmeyer–Peppas model following the empirical equation (78):

$$\log Q = \log k + n \log t$$

where Q is the drug fraction released in time t, k is a constant characteristic of the drug–polymer interaction, and n is an empirical parameter characterizing the release mechanism.

According to the diffusional exponent, RS–CS microspheres revealed n value of 0.66 ($0.85 > n > 0.43$), indicating that the release behavior followed anomalous (non-Fickian) transport where the rates of drug diffusion and polymer relaxation are comparable. Herein, the RS release was dependent on two simultaneous rate processes: both swelling-controlled and diffusion-controlled release mechanisms. Water migration into the microspheres and drug diffusion throughout the continuously swelling spheres are the combined proposed mechanisms that governed the overall release profile (79,80). n values above 0.85 indicate case II transport which is related to polymer relaxation during swelling, while n values below 0.43 indicate that drug release follows Fickian diffusion through the polymer (15,22). The obtained results were contraverse with the previous Fickian diffusion and chitosan relaxation mechanism reported by Sivadas *et al.* (81).

Verification Phase

The optimized B6 system was reprepared and the responses (Y1–Y4) were recharacterized—in triplicates—to assess the reliability of the developed optimization model. The results were compared with those determined with the multilevel factorial design. The lower magnitude of errors (−0.57, 0.7, −0.87, and 1.3) observed for mean particle size diameter, EE%, $Q_{1\ h}$, and $Q_{12\ h}$, respectively, could indicate no marked differences and/or reasonable agreements between the previous and current experimental results. It is an index of robustness and high extrapolative ability of the generated optimization model (56,82). Pursuant to the verification phase results, the B6 system was progressed for further characterization studies.

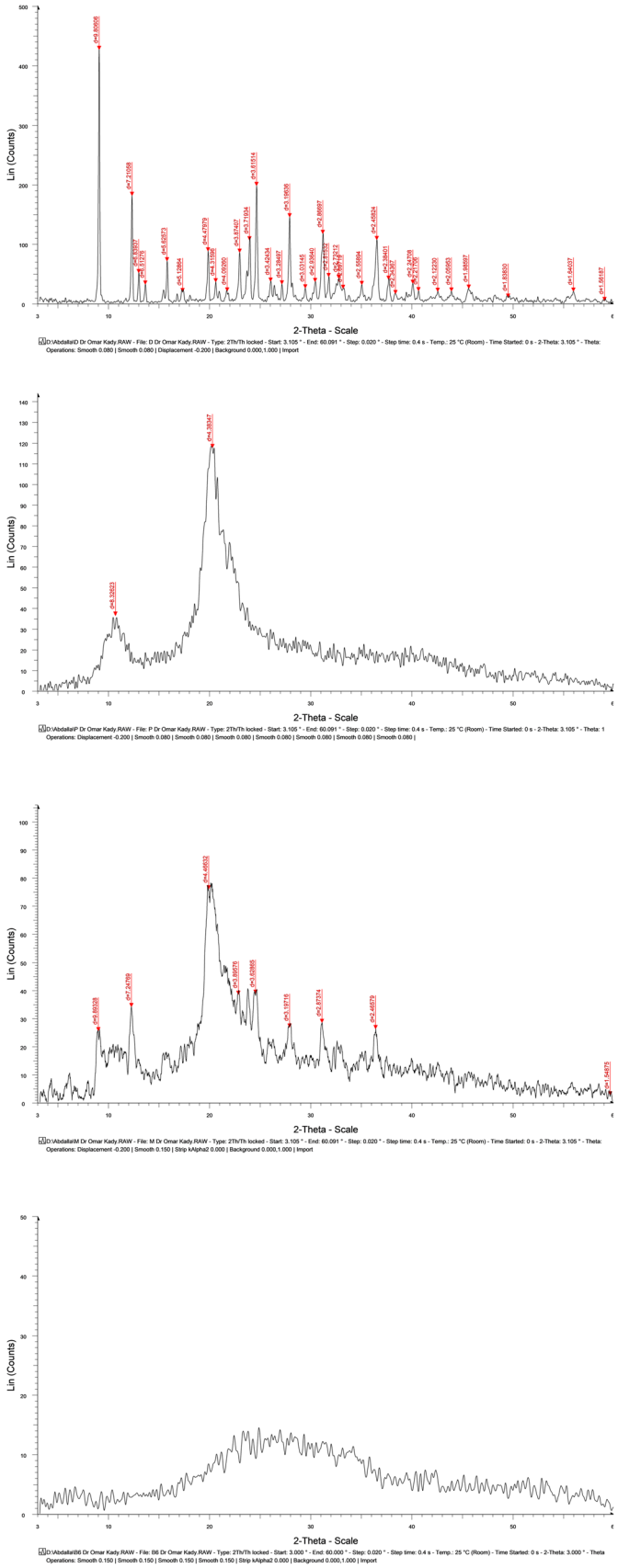

Fig. 7. XRD spectra of RS, CS, RS–CS physical mixture, and B6

TEM and Zeta Potential Measurements

TEM micrographs of the microspheres of the B6 system revealed spherical, well-identified, and discrete microspheres with an approximate size range of 3.5 ± 0.5 μm (Fig. 6) which is comparable and in good agreement with the results reported for particle size analysis using laser diffraction.

Estimation of the zeta potential of B6 microspheres revealed a high positive value of 47.9 ± 3.39 mV. This could be related to the positively charged amino groups of CS at the surface of the microspheres. Previous findings showed that zeta potential values higher than or equal to ±30 mV is required to obtain a physically stable system (83,84). It could be inferred that the observed value of the B6 system is sufficiently high to provide adequate repulsion and electrostatic stabilization between the microspheres, and hence, restrains their aggregation, as evident in TEM (85–87). This property is of great importance for RS pulmonary delivery, since the anionic nature of RS usually represents one of the main obstacles behind its poor permeability. It could be inferred that greater permeation and increase in RS cellular uptake could be granted with positively charged RS–CS microspheres (64,83,88). The cationic nature of CS is necessary for the interaction with negatively charged lung mucosa. This would be expected to promote the bioadhesion of RS microspheres at the target area in the lung until the turnover of the mucus layer, allowing the microspheres to release the therapeutic molecule over a prolonged period (89,90). Furthermore, the bioadhesion would be expected to delay the phagocytosis, the capture defense mechanism by alveolar macrophages which represents one of the major concerns of pulmonary drug delivery.

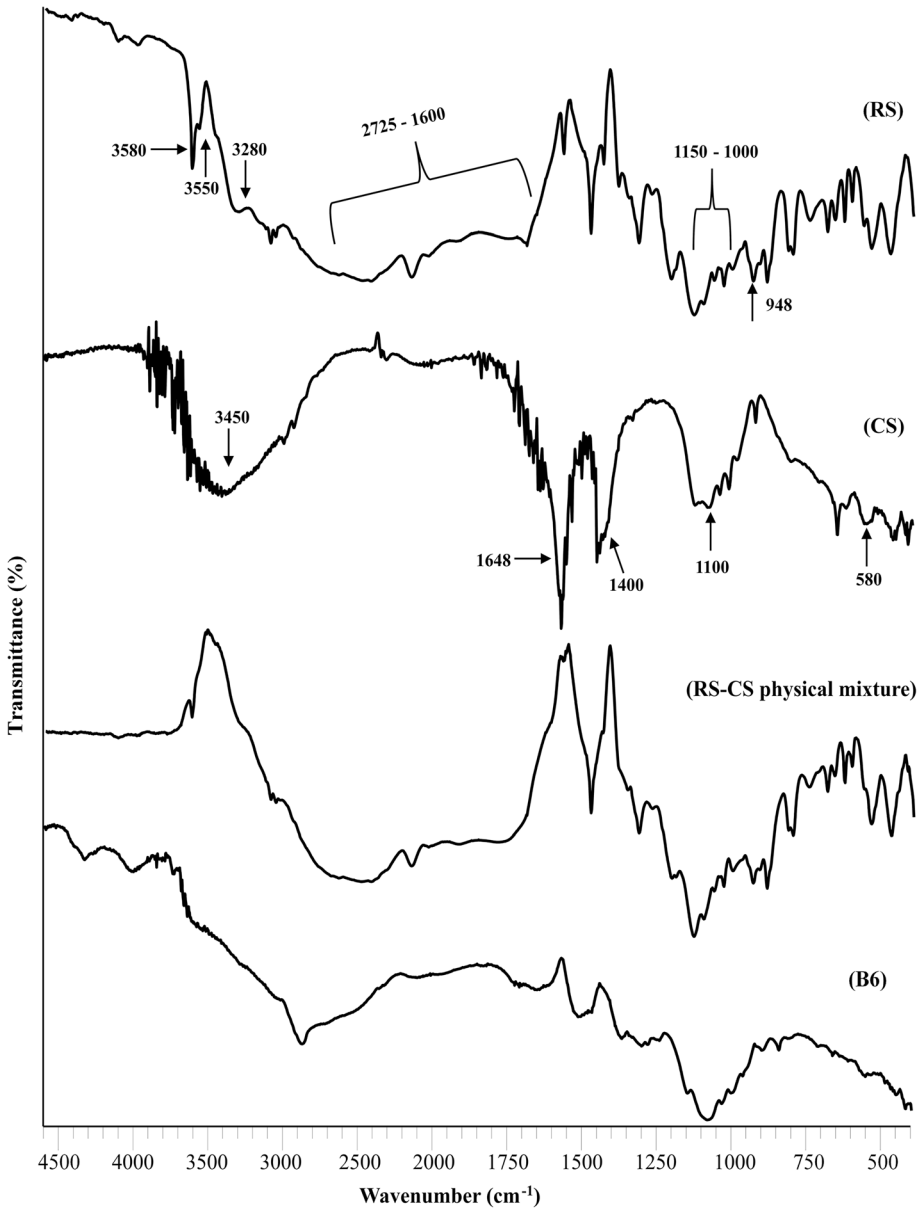

Fig. 8. FT-IR spectra of RS, CS, RS–CS physical mixture, and B6

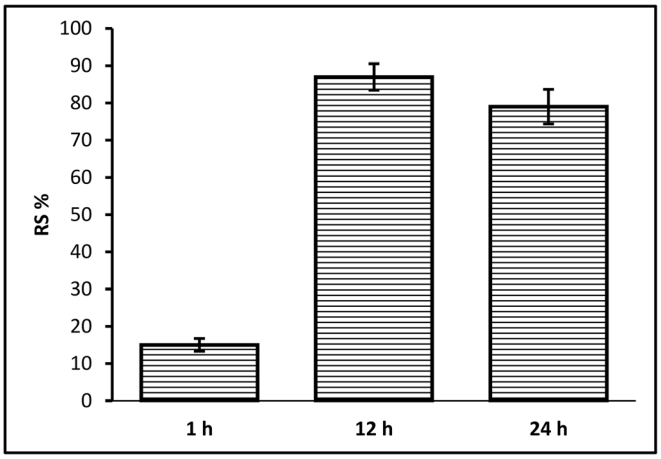

Fig. 9. Percentage of RS deposited in lung tissue along time (mean values ± SD, $n = 6$)

XRD

The physical state of RS in the microspheres of the B6 system was studied by XRD crystallography. Figure 7 displays the XRD patterns of pure RS, CS, their physical mixture, and the B6 system. Pure RS exhibited sharp and intense peaks at 2θ values of 9°, 12.2°, 24.5°, 28°, 31°, and 36.5° indicating high drug crystallinity. The diffractogram of CS showed two main distinct peaks at $2\theta = 19.8°$ related to the reflection of (2 0 0) plane and at $2\theta = 10°$ corresponding to the (0 2 0) plane, which are typical fingerprints of the semicrystalline CS (73,91,92). It was evident that although the RS–CS physical mixture has retained the main diffraction peaks of RS and CS, yet they were completely disappeared in the B6 system and the original crystallinity of the pure components has been lost. These results revealed the transformation of the crystalline RS into the amorphous state in the developed microspheres.

FT-IR

The FT-IR spectrum of RS (Fig. 8) showed two distinct −OH stretching bands at 3550 and 3580 cm^{-1}, indicative of two different water populations within the crystal lattice. The shoulder that appears at 3280 cm^{-1} is attributed to a CO–H vibration corresponding to –OH groups which are not associated with water, yet attached to the central carbon. The hydroxyl vibrations of –OH groups associated with the O=P–OH of the phosphonate group produced broad bands in the spectral region between 1600 and 2725 cm^{-1}. The characteristic bands of the phosphonate group (PO_3) were observed between 1000 and 1150 cm^{-1}, overlapping with the pyridine ring vibrations. A characteristic band for P–O was observed at 948 cm^{-1} (93).

The FT-IR spectrum of CS showed a broad absorbent band at 3450 cm^{-1} which is attributed to –OH asymmetrical stretching vibration and $–NH_2$ stretching vibration, while the band at 1648 cm^{-1} corresponds to the 1^{ry} amide groups. The absorption bands at 1400, 1100, and 580 cm^{-1} are related to the coupling of –CN– stretching vibration, –CO– stretching vibration, and –NH– stretching vibration, respectively (72). The characteristic peaks of RS and CS were maintained in the spectrum of their physical mixture, while most of them disappeared in the spectrum of the B6 system. This was clearly evident by the absence of P–O band of RS and 1^{ry} amide band of CS as well as the shifting of –OH broad bands of RS to the 2500–3000 cm^{-1} region, confirming the presence of H-bond and electrostatic interaction between RS negative hydroxyl group associated with the phosphonate group and quaternary protonated amino group ($–NH_3^+$) of CS in the B6 system prepared in weak acidic medium.

In Vivo Lung Deposition Study

To prove the potential of the developed RS–CS microspheres for pulmonary drug delivery, the *in vivo* lung deposition behavior and its persistence capacity were investigated following the intratracheal instillation of B6 microspheres at different time points 1, 12, and 24 h. It is worth to mention that the retention time of RS under the adopted chromatographic conditions was 6 min, without any interfering peaks of the tissue homogenates. Of note, the RS deposition profile in the lungs is well correlated with its *in vitro* release behavior. An initial considerable amount of RS was deposited after 1 h (15 ± 1.71%) with subsequent gradual progression in the following duration of the study. Maximum RS deposition percentage was attained at 12 h (87 ± 3.54%) post-instillation, and nevertheless, it remarkably persisted with a slight decline (79 ± 4.68%) until 24 h. This pattern is understood if one considered the time needed for RS detachment and liberation from deprotonated CS microspheres at lung pH for its deposition (Fig. 9). These findings further substantiate the importance of the cationic nature of the microspheres and their mucoadhesive potential which could be exploited to promote the lung—targeting at the main site of absorption, to reduce the microsphere clearance by

ciliary movement, and to promote the prolonged drug release (10,53,54).

CONCLUSION

In this study, RS–CS nebulizable microspheres were achieved using a systematic and risk-based QbD approach. CS was successfully used to fabricate crosslinker-free sustained release RS microspheres of respirable particle size and high EE% based on direct interionic complexation of CS cationic amino groups with negatively charged RS. In this context, the positive surface charge of the developed microspheres together with its proved persistence in the lungs up to 24 h holds promise in enhancing RS-poor transport where a reduction in the frequent dosing and the related adverse effects is anticipated. Further investigations on the potential pulmonary effectiveness and safety are currently undergoing by *in vivo* efficacy studies along with *ex vivo* safety evaluations.

COMPLIANCE WITH ETHICAL STANDARDS

The protocol of the study was reviewed and approved by the Research Ethics Committee (PI 1583) at the Faculty of Pharmacy, Cairo University (Cairo, Egypt).

Conflict of Interest The authors declare that they have no conflict of interest.

PUBLISHER'S NOTE

Springer Nature remains neutral with regard to jurisdictional claims in published maps and institutional affiliations.

REFERENCES

1. Pilcer G, Wauthoz N, Amighi K. Lactose characteristics and the generation of the aerosol. Adv Drug Deliv Rev. Elsevier. 2012;64:233–56.
2. Tan Y, Yang Z, Pan X, Chen M, Feng M, Wang L, et al. Stability and aerosolization of pressurized metered dose inhalers containing thymopentin nanoparticles produced using a bottom-up process. Int J Pharm. Elsevier. 2012;427:385–92.
3. Kaialy W, Ticehurst M, Nokhodchi A. Dry powder inhalers: mechanistic evaluation of lactose formulations containing salbutamol sulphate. Int J Pharm. Elsevier. 2012;423:184–94.
4. Wu L, Miao X, Shan Z, Huang Y, Li L, Pan X, et al. Studies on the spray dried lactose as carrier for dry powder inhalation. Asian J Pharm Sci. Elsevier. 2014;9:336–41.
5. Fleisch H. Prospective use of bisphosphonates in osteoporosis. J Clin Endocrinol Metab. Oxford University Press. 1993;76:1397–8.
6. Ueno M, Maeno T, Nishimura S, Ogata F, Masubuchi H, Hara K, et al. Alendronate inhalation ameliorates elastase-induced pulmonary emphysema in mice by induction of apoptosis of alveolar macrophages. Nat Commun. Nature Publishing Group. 2015;6:6332.
7. Panderi I, Taxiarchi E, Pistos C, Kalogria E, Vonaparti A, Panderi I, et al. Insights into the mechanism of separation of bisphosphonates by zwitterionic hydrophilic interaction liquid chromatography: application to the quantitation of risedronate in pharmaceuticals. Separations. Multidisciplinary Digital Publishing Institute. 2019;6:6.
8. Guzman ML, Soria EA, Laino C, Manzo RH, Olivera ME. Reduced food interaction and enhanced gastrointestinal tolerability of a new system based on risedronate complexed with Eudragit E100: mechanistic approaches from in vitro and in vivo studies. Eur J Pharm Biopharm. Elsevier. 2016;107:263–72.
9. Peter CP, Handt LK, Smith SM. Esophageal irritation due to alendronate sodium tablets: Possible mechanisms. Dig Dis Sci. 1998;43:1998–2002.
10. Nasr M, Awad GAS, Mansour S, Taha I. Shamy A Al, Mortada ND. Different modalities of NaCl osmogen in biodegradable microspheres for bone deposition of risedronate sodium by alveolar targeting. Eur J Pharm Biopharm. Elsevier. 2011;79:601–11.
11. Papapetrou PD. Bisphosphonate-associated adverse events. Hormones (Athens). 2009;8:96–110.
12. Nasr M, Taha I, Hathout RM. Suitability of liposomal carriers for systemic delivery of risedronate using the pulmonary route. Drug Deliv. Taylor & Francis. 2013;20:311–8.
13. Ezra A, Golomb G. Administration routes and delivery systems of bisphosphonates for the treatment of bone resorption. Adv Drug Deliv Rev. Elsevier. 2000;42:175–95.
14. Blumentals WA, Harris ST, Cole RE, Huang L, Silverman SL. Risk of severe gastrointestinal events in women treated with monthly ibandronate or weekly alendronate and risedronate. Ann Pharmacother. SAGE PublicationsSage CA: Los Angeles, CA. 2009;43:577–85.
15. Fazil M, Hassan MQ, Baboota S, Ali J. Biodegradable intranasal nanoparticulate drug delivery system of risedronate sodium for osteoporosis. Drug Deliv. Taylor & Francis. 2016;23:2428–38.
16. Pazianas M, Abrahamsen B, Ferrari S, Russell RGG. Eliminating the need for fasting with oral administration of bisphosphonates. Ther Clin Risk Manag. Dove Press. 2013;9:395–402.
17. Kim JS, Jang SW, Son M, Kim BM, Kang MJ. Enteric-coated tablet of risedronate sodium in combination with phytic acid, a natural chelating agent, for improved oral bioavailability. Eur J Pharm Sci. 2016;82:45–51.
18. Nam SH, Jeong J-H, Che X, Lim K-E, Nam H, Park J-S, et al. Topically administered risedronate shows powerful anti-osteoporosis effect in ovariectomized mouse model. Bone. 2012;50:149–55.
19. Park J-H, Jin H-E, Kim D-D, Chung S-J, Shim W-S, Shim C-K. Chitosan microspheres as an alveolar macrophage delivery system of ofloxacin via pulmonary inhalation. Int J Pharm. Elsevier. 2013;441:562–9.
20. Oyarzun-Ampuero FA, Brea J, Loza MI, Torres D, Alonso MJ. Chitosan–hyaluronic acid nanoparticles loaded with heparin for the treatment of asthma. Int J Pharm. Elsevier. 2009;381:122–9.
21. Teijeiro-Osorio D, Remuñán-López C, Alonso MJ. Chitosan/cyclodextrin nanoparticles can efficiently transfect the airway epithelium in vitro. Eur J Pharm Biopharm. Elsevier. 2009;71:257–63.
22. Debnath SK, Saisivam S, Debanth M, Omri A. Development and evaluation of chitosan nanoparticles based dry powder inhalation formulations of prothionamide. Fraceto L, editor. PLoS One. Public Library of Science. 2018;13:e0190976.
23. Foda NH, El-Laithy HM, Tadros MI. Implantable biodegradable sponges: effect of interpolymer complex formation of chitosan with gelatin on the release behavior of tramadol hydrochloride. Drug Dev Ind Pharm. 2007;33:7–17.
24. Badawi AA, El-Laithy HM, El Qidra RK, El Mofty H, El Dally M. Chitosan based nanocarriers for indomethacin ocular delivery. Arch Pharm Res. 2008;31:1040–9.
25. Pearlman O. Reviewing the use of glutaraldehyde for high-level disinfection by sonographers. J Diagnostic Med Sonogr. 2019;35:49–57.
26. Takigawa T, Endo Y. Effects of glutaraldehyde exposure on human health. J Occup Health. 2006;48:75–87.
27. Bhattarai N, Gunn J, Zhang M. Chitosan-based hydrogels for controlled, localized drug delivery. Adv Drug Deliv Rev. Elsevier. 2010;62:83–99.

28. Yu LX, Amidon G, Khan MA, Hoag SW, Polli J, Raju GK, et al. Understanding pharmaceutical quality by design. AAPS J. Springer US. 2014;16:771–83.
29. Karimi K, Pallagi E, Szabó-Révész P, Csóka I, Ambrus R. Development of a microparticle-based dry powder inhalation formulation of ciprofloxacin hydrochloride applying the quality by design approach. Drug Des Devel Ther. Dove Press. 2016;10:3331–43.
30. Amasya G, Badilli U, Aksu B, Tarimci N. Quality by design case study 1: design of 5-fluorouracil loaded lipid nanoparticles by the W/O/W double emulsion - solvent evaporation method. Eur J Pharm Sci. Elsevier. 2016;84:92–102.
31. Buttini F, Rozou S, Rossi A, Zoumpliou V, Rekkas DM. The application of quality by design framework in the pharmaceutical development of dry powder inhalers. Eur J Pharm Sci. Elsevier. 2018;113:64–76.
32. Simões A, Veiga F, Vitorino C, Figueiras A. A Tutorial for Developing a Topical Cream Formulation Based on the Quality by Design Approach. J Pharm Sci. Elsevier. 2018;107:2653–62.
33. Gyulai O, Kovács A, Sovány T, Csóka I, Aigner Z. Optimization of the critical parameters of the spherical agglomeration crystallization method by the application of the Quality by Design approach. Materials (Basel). Multidisciplinary Digital Publishing Institute (MDPI). 2018;11:635.
34. Benjasirimongkol P, Piriyaprasarth S, Moribe K, Sriamornsak P. Use of risk assessment and Plackett–Burman design for developing resveratrol spray-dried emulsions: a quality-by-design approach. AAPS PharmSciTech. 2019;20:14.
35. Kuzmov A, Minko T. Nanotechnology approaches for inhalation treatment of lung diseases. J Control Release. Elsevier. 2015;219:500–18.
36. El-Sherbiny IM, El-Baz NM, Yacoub MH. Inhaled nano- and microparticles for drug delivery. Glob Cardiol Sci Pract. Bloomsbury Qatar Foundation Journals Qatar. 2015;2015:2.
37. Shah B, Khunt D, Bhatt H, Misra M, Padh H. Application of quality by design approach for intranasal delivery of rivastigmine loaded solid lipid nanoparticles: effect on formulation and characterization parameters. Eur J Pharm Sci. Elsevier B.V. 2015;78:54–66.
38. Yerlikaya F, Ozgen A, Vural I, Guven O, Karaagaoglu E, Khan MA, et al. Development and evaluation of paclitaxel nanoparticles using a quality-by-design approach. J Pharm Sci. Elsevier. 2013;102:3748–61.
39. Pallagi E, Karimi K, Ambrus R, Szabó-Révész P, Csóka I. New aspects of developing a dry powder inhalation formulation applying the quality-by-design approach. Int J Pharm. Elsevier. 2016;511:151–60.
40. Pandey AP, Karande KP, Sonawane RO, Deshmukh PK. Applying quality by design (QbD) concept for fabrication of chitosan coated nanoliposomes. J Liposome Res. Taylor & Francis. 2014;24:37–52.
41. Ahmed OAA, Kurakula M, Banjar ZM, Afouna MI, Zidan AS. Quality by design coupled with near infrared in formulation of transdermal glimepiride liposomal films. J Pharm Sci. 2015;104:2062–75.
42. Ćurić A, Reul R, Möschwitzer J, Fricker G. Formulation optimization of itraconazole loaded PEGylated liposomes for parenteral administration by using design of experiments. Int J Pharm. Elsevier. 2013;448:189–97.
43. Xu X, Khan MA, Burgess DJ. A quality by design (QbD) case study on liposomes containing hydrophilic API: II. Screening of critical variables, and establishment of design space at laboratory scale. Int J Pharm. Elsevier. 2012;423:543–53.
44. Park S-J, Choo G-H, Hwang S-J, Kim M-S. Quality by design: screening of critical variables and formulation optimization of Eudragit E nanoparticles containing dutasteride. Arch Pharm Res. 2013;36:593–601.
45. Calvo P, Remuñán-López C, Vila-Jato JL, Alonso MJ. Novel hydrophilic chitosan-polyethylene oxide nanoparticles as protein carriers. J Appl Polym Sci. 1997;63:125–32.
46. Mennini N, Furlanetto S, Cirri M, Mura P. Quality by design approach for developing chitosan-Ca-alginate microspheres for colon delivery of celecoxib-hydroxypropyl-β-cyclodextrin-PVP complex. Eur J Pharm Biopharm. 2012;80:67–75.
47. Solaiman A, Suliman AS, Shinde S, Naz S, Elkordy AA. Application of general multilevel factorial design with formulation of fast disintegrating tablets containing croscarmellose sodium and Disintequick MCC-25. Int J Pharm. Elsevier. 2016;501:87–95.
48. Cook RO, Pannu RK, Kellaway IW. Novel sustained release microspheres for pulmonary drug delivery. J Control Release. Elsevier. 2005;104:79–90.
49. Salama RO, Traini D, Chan H-K, Young PM. Preparation and characterisation of controlled release co-spray dried drug–polymer microparticles for inhalation 2: evaluation of in vitro release profiling methodologies for controlled release respiratory aerosols. Eur J Pharm Biopharm. Elsevier. 2008;70:145–52.
50. Tadros MI, Al-mahallawi AM. Long-circulating lipoprotein-mimic nanoparticles for smart intravenous delivery of a practically-insoluble antineoplastic drug: development, preliminary safety evaluations and preclinical pharmacokinetic studies. Int J Pharm. Elsevier. 2015;493:439–50.
51. Tayel SA, El-Nabarawi MA, Tadros MI, Abd-Elsalam WH. Duodenum-triggered delivery of pravastatin sodium via enteric surface-coated nanovesicular spanlastic dispersions: development, characterization and pharmacokinetic assessments. Int J Pharm. 2015;483:77–88.
52. Stubbs C, Haigh JM, Kanfer I. Determination of erythromycin in serum and urine by high-performance liquid chromatography with ultraviolet detection. J Pharm Sci. 1985;74:1126–8.
53. Fan Y, Shan-Guang W, Yu-Fang P, Feng-Lan S, Tao L. Preparation and characteristics of erythromycin microspheres for lung targeting microspheres of erythromycin for lung targeting. Drug Dev Ind Pharm. 2009;35:639–45.
54. Pellosi DS, d'Angelo I, Maiolino S, Mitidieri E, d'Emmanueledi Villa Bianca R, Sorrentino R, et al. In vitro/in vivo investigation on the potential of Pluronic® mixed micelles for pulmonary drug delivery. Eur J Pharm Biopharm. Elsevier. 2018;130:30–8.
55. Kyriakides D, Panderi I. Development and validation of a reversed-phase ion-pair high-performance liquid chromatographic method for the determination of risedronate in pharmaceutical preparations. Anal Chim Acta. Elsevier. 2007;584:153–9.
56. Das SK, Khanam J, Nanda A. Optimization of preparation method for ketoprofen-loaded microspheres consisting polymeric blends using simplex lattice mixture design. Mater Sci Eng C. Elsevier B.V. 2016;69:598–608.
57. Kang ML, Jiang H-L, Kang SG, Guo DD, Lee DY, Cho C-S, et al. Pluronic® F127 enhances the effect as an adjuvant of chitosan microspheres in the intranasal delivery of Bordetella bronchiseptica antigens containing dermonecrotoxin. Vaccine. Elsevier. 2007;25:4602–10.
58. Vithani K, Hawley A, Jannin V, Pouton C, Boyd BJ. Inclusion of digestible surfactants in solid SMEDDS formulation removes lag time and influences the formation of structured particles during digestion. AAPS J. Springer US. 2017;19:754–64.
59. Heiskanen H, Denifl P, Pitkänen P, Hurme M. Effect of preparation conditions on the properties of microspheres prepared using an emulsion-solvent extraction process. Chem Eng Res Des. Elsevier. 2012;90:1517–26.
60. Khan MF, Ansari AH, Hameedullah M, Ahmad E, Husain FM, Zia Q, et al. Sol-gel synthesis of thorn-like ZnO nanoparticles endorsing mechanical stirring effect and their antimicrobial activities: Potential role as nano-antibiotics. Sci Rep. Nature Publishing Group. 2016;6:27689.
61. Yuan D, Jacquier JC, O'Riordan ED. Entrapment of protein in chitosan-tripolyphosphate beads and its release in an in vitro digestive model. Food Chem. Elsevier. 2017;229:495–501.
62. Moore T, Croy S, Mallapragada S, Pandit N. Experimental investigation and mathematical modeling of Pluronic® F127 gel dissolution: drug release in stirred systems. J Control Release. Elsevier. 2000;67:191–202.
63. He M, Wang H, Dou W, Chou G, Wei X, Wang Z. Preparation and drug release properties of norisoboldine-loaded chitosan microspheres. Int J Biol Macromol. Elsevier. 2016;91:1101–9.
64. Mohammed M, Syeda J, Wasan K, Wasan E. An overview of chitosan nanoparticles and its application in non-parenteral drug delivery. Pharmaceutics. 2017;9:53.

65. Ma L, Liu C. Preparation of chitosan microspheres by ionotropic gelation under a high voltage electrostatic field for protein delivery. Colloids Surf B: Biointerfaces. 2010;75:448–53.
66. Park JW, Byun Y. Ionic complex of risedronate with positively charged deoxycholic acid derivative: evaluation of physicochemical properties and enhancement of intestinal absorption in rats. Arch Pharm Res. Pharmaceutical Society of Korea. 2014;37:1560–9.
67. Jang SW, Lee JW, Ryu DS, Son M, Kang MJ. Design of pH-responsive alginate raft formulation of risedronate for reduced esophageal irritation. Int J Biol Macromol. Elsevier B.V. 2014;70:174–8.
68. Alishahi A, Mirvaghefi A, Tehrani MR, Farahmand H, Koshio S, Dorkoosh FA, et al. Chitosan nanoparticle to carry vitamin C through the gastrointestinal tract and induce the non-specific immunity system of rainbow trout (Oncorhynchus mykiss). Carbohydr Polym. Elsevier Ltd. 2011;86:142–6.
69. Ko JA, Park HJ, Hwang SJ, Park JB, Lee JS. Preparation and characterization of chitosan microparticles intended for controlled drug delivery. Int J Pharm. 2002;249:165–74.
70. Lin JH. Bisphosphonates: a review of their pharmacokinetic properties. Bone. 1996;18:75–85.
71. Bravo-Anaya LM, Soltero JFA, Rinaudo M. DNA/chitosan electrostatic complex. Int J Biol Macromol. Elsevier BV. 2016;88:345–53.
72. Rashid S, Shen C, Chen X, Li S, Chen Y, Wen Y, et al. Enhanced catalytic ability of chitosan-Cu-Fe bimetal complex for the removal of dyes in aqueous solution. RSC Adv. 2015;5:90731–41.
73. Bukzem AL, Signini R, dos Santos DM, Lião LM, Ascheri DPR. Optimization of carboxymethyl chitosan synthesis using response surface methodology and desirability function. Int J Biol Macromol. Elsevier. 2016;85:615–24.
74. Derringer G, Suich R. Simultaneous optimization of several response variables. J Qual Technol. Taylor & Francis. 1980;12:214–9.
75. El-Laithy HM, Badawi A, Abdelmalak NS, El-Sayyad N. Cubosomes as oral drug delivery systems: a promising approach for enhancing the release of clopidogrel bisulphate in the intestine. Chem Pharm Bull. 2018;66:1165–73.
76. Buratti C, Barbanera M, Lascaro E, Cotana F. Optimization of torrefaction conditions of coffee industry residues using desirability function approach. Waste Manag. Pergamon. 2018;73:523–34.
77. Ganesan P, Patil S, Pandey V, Shaju TM, Pothula S. A Practical Approach for Performing Multi-response Optimization for Advanced Process Control. Reliab Theory Appl. 2018;13:21–6.
78. Ritger PL, Peppas NA. A simple equation for description of solute release II. Fickian and anomalous release from swellable devices. J Control ReleaseElsevier. 1987;5:37–42.
79. El-Laithy HM, Nesseem DI, Shoukry M. Evaluation of two in situ gelling systems for ocular delivery of moxifloxacin: in vitro and in vivo studies. J Chem Pharm Res. 2011;3:66–79.
80. El-Laithy HM, Nesseem DI, El-Adly AA, Shoukry M. Moxifloxacin-gelrite in situ ophthalmic gelling system against photodynamic therapy for treatment of bacterial corneal inflammation. Arch Pharm Res. 2011;34:1663–78.
81. Sivadas N, O'Rourke D, Tobin A, Buckley V, Ramtoola Z, Kelly JG, et al. A comparative study of a range of polymeric microspheres as potential carriers for the inhalation of proteins. Int J Pharm. Elsevier. 2008;358:159–67.
82. Dhat S, Pund S, Kokare C, Sharma P, Shrivastava B. Risk management and statistical multivariate analysis approach for design and optimization of satranidazole nanoparticles. Eur J Pharm Sci. 2017;96:273–83.
83. Martinac A, Filipović-Grčić J, Voinovich D, Perissutti B, Franceschinis E. Development and bioadhesive properties of chitosan-ethylcellulose microspheres for nasal delivery. Int J Pharm. 2005;291:69–77.
84. Romić MD, Klarić MŠ, Lovrić J, Pepić I, Cetina-Čižmek B, Filipović-Grčić J, et al. Melatonin-loaded chitosan/Pluronic® F127 microspheres as in situ forming hydrogel: An innovative antimicrobial wound dressing. Eur J Pharm Biopharm. 2016;107:67–79.
85. Costa JR, Silva NC, Sarmento B, Pintado M. Potential chitosan-coated alginate nanoparticles for ocular delivery of daptomycin. Eur J Clin Microbiol Infect Dis. Springer. 2015;34:1255–62.
86. Peng H, Lin L, Ding G. Influences of primary particle parameters and surfactant on aggregation behavior of nanoparticles in nanorefrigerant. Energy. Elsevier Ltd. 2015;89:410–20.
87. Priyanka K, Sahu PL, Singh S. Optimization of processing parameters for the development of Ficus religiosa L. extract loaded solid lipid nanoparticles using central composite design and evaluation of antidiabetic efficacy. J Drug Deliv Sci Technol. Elsevier. 2018;43:94–102.
88. Yamamoto H, Kuno Y, Sugimoto S, Takeuchi H, Kawashima Y. Surface-modified PLGA nanosphere with chitosan improved pulmonary delivery of calcitonin by mucoadhesion and opening of the intercellular tight junctions. J Control Release. Elsevier. 2005;102:373–81.
89. Weers JG, Tarara TE, Clark AR. Design of fine particles for pulmonary drug delivery. Expert Opin Drug Deliv. 2007;4:297–313.
90. Grenha A, Al-Qadi S, Seijo B, Remuñán-López C. The potential of chitosan for pulmonary drug delivery. J Drug Deliv Sci Technol. Elsevier. 2010;20:33–43.
91. Lai C, Chen Y, Zhang S. Study on chitosan-lactate sponges with oriented pores as potential wound dressing. Mater Sci Appl. 2013;04:458–70.
92. Mukherjee D, Srinivasan B, Anbu J, Azamthulla M, Banala VT, Ramachandra SG. Improvement of bone microarchitecture in methylprednisolone induced rat model of osteoporosis by using thiolated chitosan-based risedronate mucoadhesive film. Drug Dev Ind Pharm. Taylor & Francis. 2018;44:1845–56.
93. Errassifi F, Sarda S, Barroug A, Legrouri A, Sfihi H, Rey C. Infrared, Raman and NMR investigations of risedronate adsorption on nanocrystalline apatites. J Colloid Interface Sci. 2014;420:101–11.